Binary Image Reconstruction Using Local Binary Pattern Priors

Judit Szűcs and Péter Balázs
Department of Image Processing and Computer Graphics
University of Szeged
H-6720 Árpád tér 2., Szeged, Hungary
{jszucs,pbalazs}@inf.u-szeged.hu

***Abstract*—We provide a novel approach for binary image reconstruction using few projections. The inherently insufficient amount of projection data is augmented by statistical image priors describing the approximate texture of the image to reconstruct. The priors are extracted from sample images, in advance of the reconstruction. Experimental results on software phantom images show that this approach can be a useful alternative of former reconstruction methods as, under certain circumstances, it provides better image quality.**

***Keywords*-binary tomography, image reconstruction, local binary pattern, simulated annealing**

I. Introduction

The basic aim of image reconstruction is to create 2D images from their sets of line integrals (in the discrete case, line sums) taken along parallel lines in different directions. A collection of line sums taken from the same direction is called a *projection* of the image. When only few projections are available the reconstruction is usually underdetermined, thus many significantly different solutions of the same task can exist. One way to overcome this problem is to incorporate prior information into the reconstruction process and to reduce the search space of feasible solutions. A special case is when the object to reconstruct consists of a single material yielding that the image representing the object is binary. This is in main focus in *Binary Tomography* (BT) which has important applications in crystallography, materials science, and industrial non-destructive testing, just to mention a few [1], [2].

There is a wide literature of image reconstruction algorithms in BT using different kinds of geometrical or shape priors, depending on the application. In this paper we investigate a novel prior, a Local Binary Pattern (LBP) texture descriptor to improve the quality of the reconstruction. LBP feature vectors are used to represent image textures, extracted from images of different classes. During the reconstruction we use these features to force the reconstructed image to have a texture similar to the observed ones. Such a method can be useful when there are sample images which are structurally similar to the one to reconstruct, a common scenario in industrial tomography applications. The paper presents our preliminary experiences.

The paper is structured as follows. Section II is a short overview of the existing image reconstruction methods. In Section III we present our algorithm. In Section IV we report on experimental results. Finally, Section V is for the conclusions.

II. Reconstruction Algorithms

A. Analytical Methods

Analytical reconstruction methods (see, e.g., in [3]) are based on the observation that the 1D Fourier transform of a projection function corresponds to a line of the 2D Fourier transform of the original image. Therefore, taking sufficiently many projections can determine the 2D Fourier transform of the image to reconstruct, and thus the image itself. Analytical methods are fast and accurate, and therefore they are widely used in medical CT-scanners. However, they need several hundreds of projections to achieve reasonable image quality, thus they are almost always useless when only few projections are available.

B. Algebraic Reconstruction Methods

Algebraic reconstruction techniques can provide good reconstructions even when the number of projections is limited. They formulate the reconstruction problem as a linear system of equations and use iterative methods to solve this system. Due to physical limitations showing up in practice (scanner constraints, noisy projections, etc.) usually just an approximate solution is found. The difference of these methods lies in the diversity of the approximation method.

The basic iterative process is the ART (Algebraic Reconstruction Technique), which interprets the equations as hyperplanes and uses Kaczmarz's algorithm to approach the "intersection" of these planes [4].

DART (Discrete Algebraic Reconstruction Technique) is based on the above technique taking advantage of the properties of the discrete images: the range of image function is finite and contains just a small number of elements [5]. Thresholding the result of an arbitrary continuous reconstruction method gives usually an approximately good result even for the discrete task, except that it is inaccurate at the boundary of the object in the image. Therefore, after performing and thresholding ART, DART refines the boundary step-by-step in each iteration according to the current and the measured projection data. DART is robust against the errors generated during the estimation of the gray values and it also can

treat noisy projections. It is one of the most effectively used algorithm in the field of Binary Tomography.

C. Binary Reconstruction by Optimization

Binary Tomography is a special case of discrete tomography where the image pixels to reconstruct can only take two values: 0 or 1. Using this prior information the binary reconstruction can be traced back to the equation known from algebraic reconstruction $\mathbf{Ax} = \mathbf{b}$, where the $\mathbf{A}$ matrix describes the relationship between the beams and pixels (a_{ij} gives the length of the line segment of the i-th projection ray in the j-th pixel), vector $\mathbf{b}$ contains the measured projection values, and $\mathbf{x} \in \{0,1\}^{mn}$ represents the unknown image of size $m \times n$, in a row-by-row vector form. To facilitate the difficulties arising from the size and underdeterminedness of the system, from binary variables, and measurement errors, this task is often reformulated to the problem of minimizing

$$C(\mathbf{x}) = ||\mathbf{Ax} - \mathbf{b}||^2 + \gamma \cdot \Phi(\mathbf{x}) \ , \tag{1}$$

where $||\mathbf{Ax} - \mathbf{b}||^2$ ensures that the projections of the reconstructed image are close to the measured ones (data fitting term), and $\Phi(\mathbf{x}) : \{0,1\}^{mn} \to \mathbb{R}$ measures how well the reconstructed image fits the prior information accessible (e.g., homogeneity, convexity, circularity, etc.). Finally $\gamma \geq 0$ is a scaling constant. To solve this binary optimization problem one can choose an arbitrary suitable global optimizer.

III. Reconstruction with LBP Priors

Using Local Binary Patterns (LBP) is a good way to find image patterns or repetitions [6]. LBP is a type of visual descriptor for classification in computer vision. Primarily, it is used to describe the texture by representing the relationship between each pixel and its 8-neighbors with a binary code. Each of the 8-neighbors can have smaller or non-smaller value than the center pixel. Thus, there are 256 such binary codes, and as a result of a basic LBP process we gain a 256-dimensional feature vector describing the normalized distribution of the binary codes in the image. LBP can be used by arbitrary image classification machine learning algorithm. We apply it to optimize the reconstruction.

Assuming that the image to reconstruct can belong to one of k given classes we first choose representatives of those classes and calculate their LBP vectors. Then, in the reconstruction we take two priors into account. First, the image should be smooth, and second, it must have a texture similar to the previously observed ones. Having two different priors, the formula of (1) becomes

$$C(\mathbf{x}) = ||\mathbf{Ax} - \mathbf{b}||^2 + \gamma_1 \cdot \Phi_1(\mathbf{x}) + \gamma_2 \cdot \Phi_2(\mathbf{x}) \ , \tag{2}$$

where $\Phi_1(\mathbf{x})$ measures the smoothness of the current solution by taking the sum of the convolution of each image pixel by a Gaussian-like kernel and $\Phi_2(\mathbf{x})$ gives the minimal Euclidean distance of the LBP vector of the current image compared to all representative LBP vectors. Again, γ_1 and γ_2 are scaling weights.

IV. Experimental Results

A. Implementation Details

To optimize cost function (2) we used simulated annealing (SA) [7]. The parameters of (2) and the SA algorithm were set manually. We found that the best parameter values for (2) were $\gamma_1 \in [0.03, 0.06]$ and $\gamma_2 = 0.5$ having a convolution mask

$$\frac{1}{\sqrt{2\pi}} \begin{pmatrix} 0 & 0 & e^{-2} & 0 & 0 \\ 0 & e^{-\sqrt{2}} & e^{-1} & e^{-\sqrt{2}} & 0 \\ e^{-2} & e^{-1} & 0 & e^{-1} & e^{-2} \\ 0 & e^{-\sqrt{2}} & e^{-1} & e^{-\sqrt{2}} & 0 \\ 0 & 0 & e^{-2} & 0 & 0 \end{pmatrix} .$$

The SA started each time from a random image and in each iteration some of the image pixels were randomly chosen and inverted (the number of such pixels depended on the actual value of the cost function). The stopping criteria of the algorithm was to reach 800.000 iterations or to perform 50.000 iterations without improving the optimal result. As a comparison, we also reconstructed the images by the DART algorithm. To calculate the LBP vectors we used the source-code of [8]. All the algorithms were implemented in MATLAB.

B. Results

To test the efficiency of our method we conducted experiments on software phantom images arising from 6 classes with different textures. Figure 1 shows representatives. Images in Class 1 are formed by shapes with four possible orientations resembling regular patterns. These images were introduced as basic phantoms, due to their strict structure. Class 4 contained similar images but with bigger empty areas between them, to study if the size of the objects affects the reconstruction quality. Classes 2, 5, and 6 consisted of images showing regular or less regular patterns of circular holes having equal or different sizes. Such images are typical in industrial non-destructive testing where the aim is to detect air bubbles in homogenous objects (e.g. cheese, chocolate, but also metal alloy products). Furthermore, by interchanging the foreground and background, the holes become small "particles" thus providing structures similar to observe in electronmicroscopic tomography of crystalline structures. Finally, images in Class 3 (or more precisely, their inverted versions) show thin walls between similar objects. These images can remind us to cross-sections of trabecular bones or metal- or plastic foams. Each class contained 150 images of size 64×64 for extracting the reference LBP values, and additional 10 images for testing. To determine the quality of the reconstruction we used RME (Relative Mean Error) error rate:

$$RME = \frac{\sum_i |f_i^o - f_i^r|}{\sum_i f_i^o} \cdot 100\% \ , \tag{3}$$

were f_i^o and f_i^r stand for the i-th pixel of the original and reconstructed image, respectively. Obviously, the lower is the value the better the result is. Note, that it also can happen that RME is greater than 100%. The reconstructions were performed from 2, 3, 4, and 8 projections assuming parallel

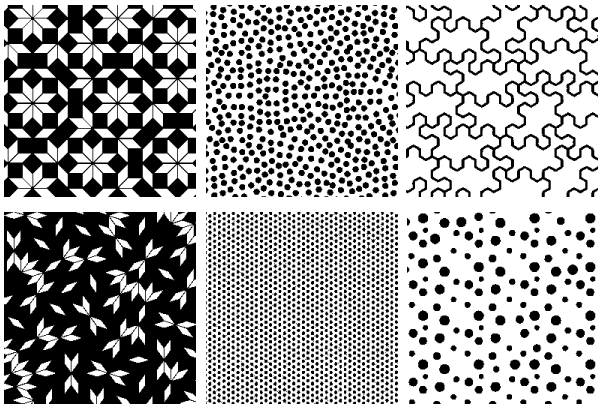

Fig. 1. Test phantom images. Representative images of Class 1-6 from left to right and top to bottom, respectively.

beam geometry with one pixel distance between the projection lines. Due to the stochastic nature of SA each reconstruction task was repeated 5 times and the average values of the results were taken.

For space considerations we only report here RME values for two classes of images. The remaining image classes yield more or less similar results. Table I (Table II) collects the results for Class 1 (resp. Class 6). The better values are highlighted. From the entries of these tables (and of the further tables not presented here) we can deduce the following. The proposed method behaves similarly for Classes 1-5. Namely, in case of 2 or 3 projections SA may achieve better results than DART. Using 4 or 8 projections, SA does not perform better, but usually the differences are not significant. Exceptions are Classes 2 and 4, for which the differences in case of 8 projections are bigger. Interestingly, the results of Class 6 with 2, 3, and 4 projections are similar for both SA and DART, but with 8 projections SA often provides better results or even perfect reconstructions (0% RME).

Figure 2 shows one example of how the RME value changes for the same test image (a member of Class 1, in this case) if the number of projections is increased. It clearly reveals that the trend is similar for the two algorithms. This graph is also a good example for an RME value greater than 100%. Furthermore, it can be seen that in this case SA gave better results for 2 and 8 projections. When using 20 projections, both algorithms resulted in perfect reconstructions.

Regarding the running times, we observed that SA usually terminated after 100.000-200.000 iterations in about 3-6 minutes. Unfortunately, there are also image classes (e.g., Class 5) for which SA may need up to 20 minutes to finish the reconstruction. This is much slower than DART which usually runs in less than a minute. However, the code has not been optimized yet, thus we expect significant improvements, from that point of view.

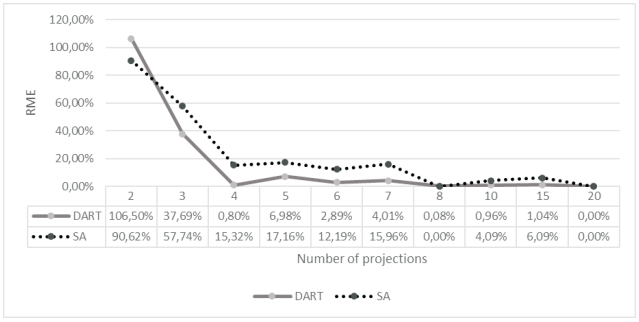

Fig. 2. Example of how the RME value changes by increasing the number of projections (dots are connected for better visibility).

V. Conclusions

In this paper we presented a method which tries to reconstruct an element of a specified class of binary images using the gathered prior data about the texture of the image. As a texture descriptor we used the basic LBP feature. Performing experimental analysis of software phantom images we found that the concept is promising (especially in case of few projections). We presented here our preliminary results. Unfortunately, the fine-tuning of the parameters is not perfect yet. One of our future plans is to find better settings for these parameters. Although the running time of the algorithm is also not satisfying yet, it could be significantly decreased with code optimization. One advantage of our method is that it could be evolved by using other versions of LBP, or further texture descriptors. Also, SA can be replaced with other global optimizers. Finally, the method seems to be easy to extend to multivalued discrete or general greyscale image reconstruction, too. In summary, our idea proved to be successful and we see a lot of options to improve its practical applicability.

Acknowledgment

This work was supported by the NKFIH OTKA K112998 grant.

References

[1] G.T. Herman, A. Kuba (Eds.), Discrete Tomography: Foundations, Algorithms and Applications, Birkhäuser, Boston, 1999.
[2] G.T. Herman, A. Kuba (Eds.): Advances in Discrete Tomography and Its Applications. Birkhäuser, Boston, 2007.
[3] A.C. Kak, M. Slaney, Principles of Computerized Tomographic Imaging, IEEE Press, 1988.
[4] R. Gordon, R. Bender, G.T. Herman: Algebraic reconstruction techniques (ART) for three-dimensional electron microscopy and x-ray photography. Journal of Theoretical Biology 29 (1970) 471–481
[5] K.J. Batenburg, J. Sijbers: DART: A practical reconstruction algorithm for discrete tomography, IEEE Trans. on Image Processing 20 (2011) 2542–2553
[6] T. Ojala, M. Pietikäinen, T. Mäenpää: Multiresolution gray-scale and rotation invariant texture classification with Local Binary Patterns. IEEE Trans. on Pattern Analysis and Machine Intelligence 24 (2002) 971–987.
[7] S. Kirkpatrick, C.D. Gelatt, M.P. Vecchi: Optimization by Simulated Annealing. Science 220 (1983) 671–680.
[8] Center for Machine Vision Research, University of Oulo (`http://www.cse.oulu.fi/CMV`)

TABLE I
RME VALUES IN PERCENT FOR THE 10 TEST IMAGES IN CLASS 1

	2		3		4		8	
	SA	DART	SA	DART	SA	DART	SA	DART
1	71.18	**66.23**	47.84	**33.50**	11.13	**3.18**	2.95	**0.05**
2	**64.61**	65.59	**62.50**	65.03	15.40	**0.56**	1.61	**0.12**
3	**42.97**	43.82	39.95	**23.32**	10.38	**0.26**	3.13	**0.05**
4	**68.60**	72.97	44.21	**36.46**	12.41	**2.41**	3.58	**0.50**
5	66.75	**66.55**	30.93	**22.22**	8.26	**1.85**	4.64	**1.08**
6	**81.84**	106.50	58.85	**37.69**	19.97	**0.80**	0.26	**0.08**
7	85.02	**74.84**	**48.71**	49.32	13.80	**4.63**	0.38	**0.07**
8	**59.91**	71.00	45.81	**29.83**	18.94	**0.95**	3.12	**0.12**
9	69.28	**40.50**	55.50	**33.31**	21.39	**1.13**	1.90	**0.74**
10	77.28	**71.84**	44.07	**26.24**	11.69	**9.58**	1.15	**0.20**

TABLE II
RME VALUES IN PERCENT FOR THE 10 TEST IMAGES IN CLASS 6

	2		3		4		8	
	SA	DART	SA	DART	SA	DART	SA	DART
1	24.41	**22.50**	14.39	**1.59**	14.14	**0.41**	**0.00**	0.03
2	30.88	**27.02**	24.88	**16.92**	18.83	**18.35**	**0.00**	0.06
3	27.93	**24.74**	19.98	**17.27**	**20.74**	20.81	**0.00**	0.09
4	**28.00**	36.70	14.30	**10.81**	15.77	**2.02**	**0.02**	0.03
5	24.88	**17.73**	14.05	**7.23**	13.70	**3.67**	2.29	**1.08**
6	**29.07**	30.91	15.42	**10.71**	17.72	**13.40**	**0.02**	0.21
7	**27.52**	35.45	20.64	**2.18**	15.74	**0.92**	**0.00**	0.12
8	**34.14**	38.94	24.96	**22.37**	16.69	**10.62**	0.55	**0.12**
9	**27.51**	34.06	18.32	**9.52**	19.43	**4.13**	**0.00**	**0.00**
10	**33.11**	37.20	23.07	**2.68**	25.03	**20.54**	**0.00**	0.31